I&EC research
Industrial & Engineering Chemistry Research

Article

pubs.acs.org/IECR

The Particle Removing Characteristics in a Fixed Valve Tray Column

Qingli Wang,[†,‡] Xueli Chen,*[,†,‡] and Xin Gong[†,‡]

[†]Key Laboratory of Coal Gasification and Energy Chemical Engineering of Ministry of Education, East China University of Science and Technology, Shanghai 200237, P.R. China

[‡]Shanghai Engineering Research Center of Coal Gasification, East China University of Science and Technology, Shanghai 200237, P.R. China

ABSTRACT: A method of predicting the particle collection efficiency of a fixed valve tray column and the particle size distribution properties, which considers diffusion, interception, and impaction, is presented to study the particle removal mechanisms of a fixed valve column. The particle size distribution of fly ash particles is represented by a log-normal function, and the continuous evolution of the particle size distribution in a fixed valve column is taken into account with the first three moment equations. The results show that the collection efficiency is represented as a U-shaped curve with a minimum in the region of around 2.0 μm in particle size. This allows fly ash particles in the diffusion and in the impaction-dominant regions to be removed at a higher rate compared with fly ash in the intermediate region. As particles pass through the bubble column, the geometric standard deviations of the size distribution of fly ash particles decrease. The geometric mean diameter of fly ash particles in the diffusion-dominant region increases, whereas it decreases in the impaction-dominant region. The present study also shows that, in optimum operation conditions such as low bubble slip velocity, small bubble size, and high gas holdup, the fixed valve tray column has sufficient ability to remove tiny and hydrophobic particles.

1. INTRODUCTION

One of the major technological hurdles with the commercialization of advanced gasification based power and hydrogen production systems is an unreliable gas cleaning process.[1] The raw syngas from the coal gasifier contains a number of solid and fluid contaminants which have to be removed at the highest possible in order to protect downstream process equipment and catalysts. Unlike the syngas purification in GE gasification technology, in the OMB (the opposed multiburner) gasification purification process, a combination of mixer, cyclone, and tray column scrubber is adopted.[2] Cyclones are widely used because of their low costs of installation, operation, and maintenance. However, their particle collection efficiency rapidly decreases with decreasing particle size,[3,4] so that a bubble column is adopted for deeper purification of syngas; the goal is to control the content of fly ash below 1 mg/Nm^3 in syngas.[5]

Figure 1 is a schematic of a fixed valve tray column scrubber. The unit causes very little pressure loss and can handle large volumes of gases. As the particle-laden gas flows upward, particles collide with the bubble surface, and then, liquid containing the particles is withdrawn at the bottom of the bubble column. It is known that a normal bubble column is generally not suitable for removing particles smaller than 1.0 μm due to the limitations of the specific interfacial area α. A bubble column combined with a cyclone[6] and a modified multistage bubble column[7] have been suggested as two of the primary means to increase small particle removal efficiency. However, the exact mechanisms involved and the change of particle size distribution are still not fully understood. Despite the importance of understanding the fly ash particle removal processes in bubble column,[8−11] no systematically parameterized study to define the scavenged particle distributions, as a function of particle properties and bubble size, has been established.

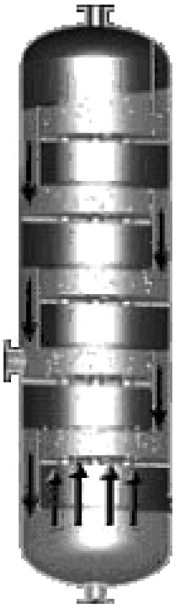

Figure 1. A schematic of the fixed valve tray column scrubber.

This study primarily seeks to present the particle removing characteristics of a fixed valve tray column scrubber by exploring the effects of several variables numerically, such as bubble size, relative velocity of bubble and liquid, gas holdup, particle size, and wettability. In addition, the moment method is used for predicting not only the particle collection efficiency of

Received: October 8, 2012
Revised: January 22, 2013
Accepted: February 10, 2013
Published: February 11, 2013

dx.doi.org/10.1021/ie3027422 | *Ind. Eng. Chem. Res.* 2013, 52, 3441−3452

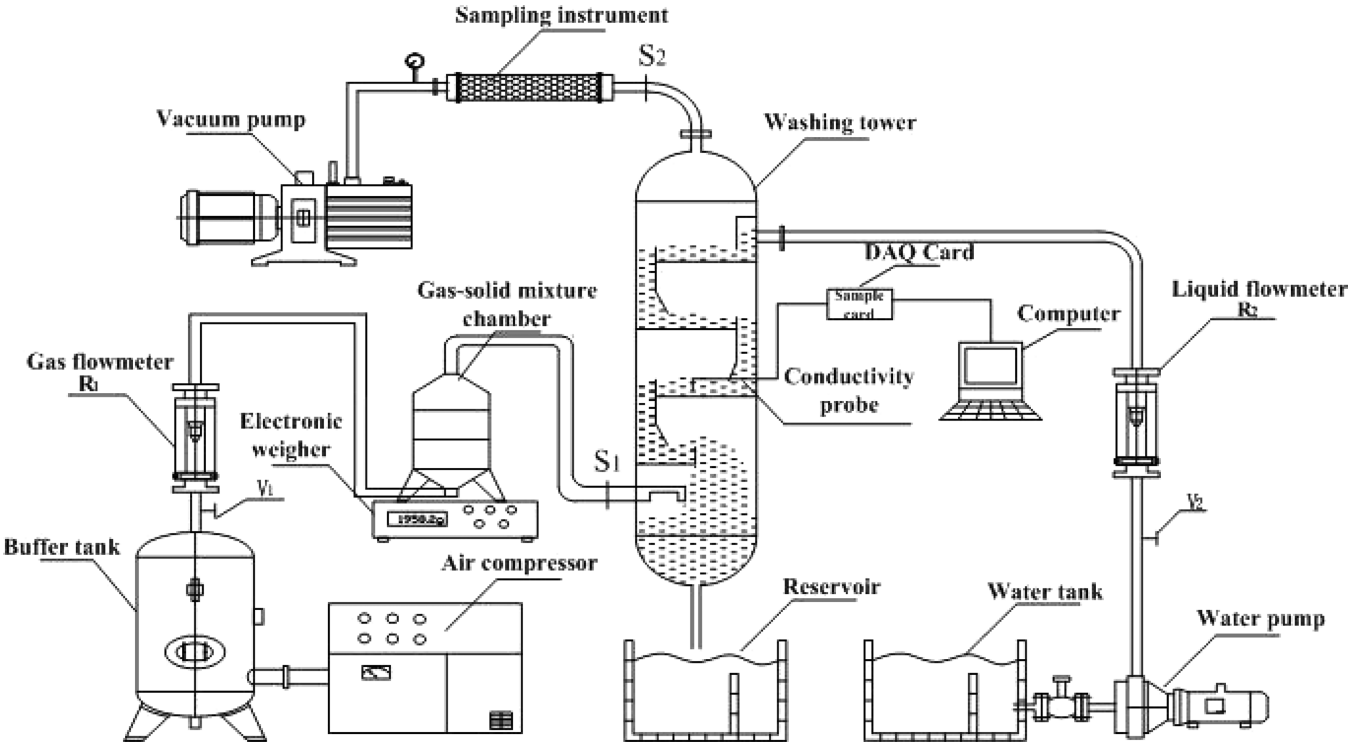

Figure 2. A schematic of the system measuring the particle collection efficiency of fixed valve tray column scrubber.

the fixed valve tray column but also the particle size distribution properties. This method takes into account diffusion, impaction, and interception. It is assumed that three collection efficiencies are additive, so the collection efficiency is described as the sum of all three. The approach also assumes that the size distribution of fly ash particles initially manifesting a log-normal distribution has three size parameters of a log-normal distribution function as the fly ash passes along the tray column. A log-normal distribution function is described by three parameters. The three size distribution parameters, namely, the mean particle diameter, the geometric standard deviation, and the total particle number, are allowed to change during the calculation. The numerical results were compared with experimental results.

2. EXPERIMENTAL SETUP

2.1. Apparatus, Materials, and Method. Experiments to determine the effect of particle diameter and material, gas flow rate, liquid flow rate, and gas holdup on collection efficiency were carried out on a test apparatus, as shown in Figure 2. The experimental bubble scrubber is a vertical cylindrical Perspex column, 90 mm in diameter and 1350 mm long. The basic components of this apparatus were

(a) fixed valve tray column

(b) fine particle generator

Auxiliary equipment included the air flow systems, water flow systems, the associated controlling and measuring devices, as well as instruments for measuring particle concentration.

The structure of the fixed valve tray is shown in Figure 3. The vertical Perspex column has been constructed in three vertical stages, which, in effect, operate in series.

The tray structural parameters are shown in Table 1.

Two different types of particles were used:

Figure 3. The fixed valve tray.

Table 1. Fixed Valve Tray Configuration Parameter

parameter	value
the ratio of perforation area to tray area, ϕ (%)	11.8
diameter of fixed valve, D (mm)	25
fixed valve height, H (mm)	6
Weir height, h_w (mm)	50
Weir length, l_w (mm)	84

Glass beads, 0.275−158.485 μm, contact angle 21.5°, circular degree 0.95, ρ_p = 2.5 g/cm^3

Fly ash particles, 0.275−158.485 μm, contact angle 47°, circular degree 0.91, ρ_p = 1.85 g/cm^3

The fly ash particles used in the study were collected from an opposed multiburner (OMB) gasification system in Jiangsu Linggu Chemical Co, LTD, Jiangsu Province, China. The glass beads used in this study were supplied by Jichuan Co, LTD, Shanghai, China. The size distribution of fly ash particles was analyzed by a particulate size analysis system (model: MS2000, Malvern, U.K.). The original size distributions of two kinds of particles are plotted in Figure 4. The sizes of the particles

dx.doi.org/10.1021/ie3027422 | Ind. Eng. Chem. Res. 2013, 52, 3441−3452

ranged from 0.275 to 158.485 μm, close to Gaussian distribution.

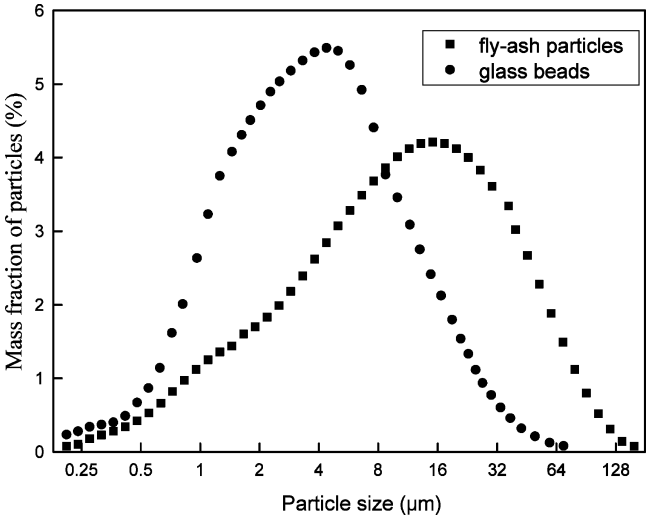

Figure 4. Typical particle size distribution of fly ash and glass beads at the inlet of a fixed valve tray column scrubber.

2.2. Experimental Procedure. The air−particle mixture was generated by mixing air and particles in a gas−solid mixture chamber. Compressed air from the compressor was used as the motive fluid in the gas−solid mixture chamber to blow and thoroughly mix air with particles in the gas−solid mixture chamber, and the mixture was fed into the bottom of the washing column.

In the actual experiment, water was continuously fed at the top of the column through a valve and rotameter and withdrawn at the bottom at such a rate that a particular liquid height and bubble volume gas−liquid dispersion volume can be maintained in the column. In order to collect representative samples, particle samples were withdrawn completely.

The fly ash was kept in the gas−solid mixture chamber aided by an electric vibrator for mixing the solids well with the air stream and was sent with gases from the bottom of the column with the flow rates ranging from 4 to 7 m^3/h. The concentrations of particulates in the inlet and outlet sampling points (S1 and S2) were measured by using a glass filter medium (99% or higher efficiency for particles 0.3 μm or larger in diameter). The fly-ash-laden gas was sampled at the source points S1 and S2 with the help of a glass fiber filter paper mounted on an assembly for holding the filter paper. A controlled volume of gas was allowed to pass through the filter paper using an aspirator filter pump. The iso-kinetic conditions were maintained during sample collection. The particles collected on the filter paper were dried at 378 K in a drying oven and cooled in desiccators. The difference in weight of the filter paper containing fly ash particles and the filter paper previously weighed alone gave the total mass of particles collected. The size distribution of fly ash particles was analyzed by a particulate size analysis system (model: MS 2000, Marlvern, U.K.). The results were quite reproducible, and each data point in the figures represents an average of several measurements. The standard deviation of the samples for any given point was usually smaller than 10% of the median (closer to 7%).

Experiments have been conducted with liquid flow rates of 160−280 L/h. Corresponding to liquid flow rate, gas flow rates of 4−7 m^3/h were used. The scrubbing liquid in these sets of experiments was water. The collection efficiency of fly ash has been calculated for each run by the formula as follows:

(1) Overall collection efficiency

The difference in weight of the filter paper containing particles and the filter paper previously weighted alone gave the total mass of particles collected. The total efficiency of the scrubber in particulate separation, E_T, was determined gravimetrically as follows:

$$E_T = 1 - \frac{m_{out}}{m_{in}} \quad (1)$$

where m_{out} is the mass of unseparated particles in exit air retained on the filter (g) and m_{in} is the mass of particles fed into the scrubber (g).

(2) Grade efficiency

The grade efficiency was calculated using the following equation:

$$G(x) = 1 - (1 - E_T)\frac{\omega_{out,x}}{\omega_{in,x}} \quad (2)$$

where $\omega_{out,x}$ is the mass fraction of unseparated particles in exit air retained on the filter at particle size x and $\omega_{in,x}$ is the mass fraction of particles fed into the scrubber at particle size x.

3. THEORETICAL MODELING OF WASHING COLUMN

3.1. Basic Assumptions. The following major assumptions are made in developing the proposed model to study the prediction for performance of the fixed valve tray column:

(1) No loading occurs on the bubbles, and the particles adhere to the bubble surface upon contact.
(2) Air follows the ideal gas law.
(3) Bubbles and particles are spherical.
(4) Bubble size distribution is uniform.

3.2. Mass Balance Equation. When particle-laden gas passes up through a water layer on the tray, a number of small air bubbles are formed. In a process called bubble scrubbing, fly ash particles entrained in bubbles rising through the gas−water mixture on the tray were collected on the bubble surface due to various transport mechanisms including Brownian diffusion, interception, and inertial impaction. Brownian diffusion controls the removal rate for small particles, whereas inertial impaction plays significant roles for large particles. Even if the trajectory of a particle does not depart from the streamline, a particle may still be collected when the center of the particle passes within one particle radius from the bubble surface. If significant evaporation or condensation takes place, Stefan flow can impose an additional aerodynamic impact on the motion of particles. In this study, this effect is neglected.

A mathematical model based on mass balance has been developed over a control volume of the fixed valve column. Applying the mass balance equation to a cylindrical element of height dz taken inside the fixed valve column, as shown in Figure 5, the following equation is obtained[12]

$$-\frac{Q_G}{A_c}\,dc = \frac{6Q_G}{\pi {d_b}^3 A_c}\cdot\frac{dz}{v_b}\cdot\frac{\pi {d_b}^2}{4}\cdot U\cdot c\cdot\eta_s \quad (3)$$

where Q_G is the gas flow rate (m^3/s), A_c the tray bubbling area (m^2), U the relative velocity between bubbles and liquid (m/s),

dx.doi.org/10.1021/ie3027422 | Ind. Eng. Chem. Res. 2013, 52, 3441−3452

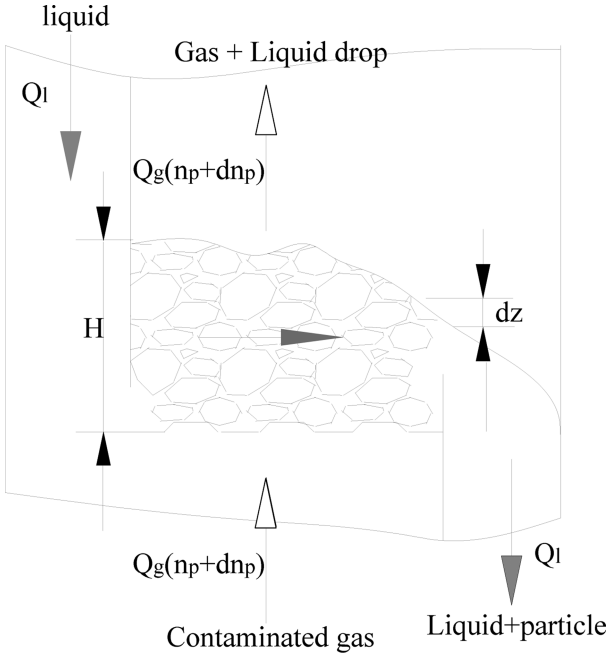

Figure 5. Schematic of a fixed valve tray column.

c the particle concentration in a bubble (g/m^3), η_s the fraction of particles collected in a bubble, d_b the Sauter mean bubble diameter (m), and v_b the bubble rise velocity (m/s).

$$\frac{dn}{dz} = -\frac{3}{2}\cdot\eta_s\frac{U}{d_b v_b}\cdot n \tag{4a}$$

Equation 4a is derived using eq 3 and can be rewritten as the following form in terms of the particle collection taking place at a particular time.

$$\frac{dn}{dt} = -\frac{3}{2}\cdot\eta_s\frac{U}{d_b}\cdot n = -A\cdot\eta_s n \tag{4b}$$

where

$$A = \frac{3}{2}\cdot\frac{U}{d_b}$$

Equation 4a can be integrated over the froth height on the tray, H_F, to yield eq 5.

$$\frac{n}{n_0} = \exp\left\{-\frac{3}{2}\cdot\eta_s\frac{U}{v_b}\cdot\frac{H_F}{d_b}\right\} \tag{5}$$

Hence,

$$\eta_{total} = 1 - \frac{n}{n_0} = 1 - \exp\left\{-\frac{3}{2}\cdot\frac{U}{v_b}\cdot\frac{H_F}{d_b}\cdot\eta_s\right\} \tag{6}$$

3.3. Model Parameter Estimation. The model equations developed on the basis of mass balance, described in the previous section, contain a number of independent hydrodynamic and transport parameters. These parameters determine the performance of the tray column scrubber. The best correlation available in the literature for these parameters has been given below.

3.3.1. Gas Holdup. The froth height and clear liquid height are useful in calculating bubble residence times, gas holdup, and collection efficiency. The froth height has been involved in many research papers, and it is mainly affected by the tray geometry, gas, and liquid flow rate.[13] In the present work, the clear liquid height and froth height were experimentally determined to calculate the gas holdup using eq 7.

$$\varphi_g = (H_F - H_0)/H_F \tag{7}$$

where φ_g is the gas holdup, H_0 the clear liquid height, and H_F the froth height.

3.3.2. Bubble Size in Fixed Valve Tray Column. The bubble size is measured through the double-sensor conductivity probe[14] and calculated by applying the statistical method of sampling. The Hesketh[15] and Liang[16] empirical equation was used for theoretical analysis of the bubble diameter:

$$d_b = \beta\cdot\left(\frac{\sigma}{\rho_L}\right)^{3/5}(u_g g)^{-2/5} \tag{8}$$

where

$$\beta = \frac{C_n}{C_d^{2/5}}\cdot\left(\frac{We_c}{2}\right)^{3/5}$$

$0 < C_d < 1$ is the percentage of energy dissipation that is dependent on the tray configurations, and C_n is the ratio of the sauter mean bubble diameter (d_b) and the maximum stable bubble (d_{max}).

3.3.3. The Bubble Rise Velocity in a Fixed Valve Tray Column. Although the velocity of any individual bubble in the dispersion cannot be predicted with any certainty, the mean velocity of a sample of many bubbles of a given size is a reproducible quantity which is significantly related to the bubble superficial gas velocity and gas holdup. The bubble rise velocity is calculated from the following relationship[17]

$$v_b = u_g/\varphi_g - u_l/\varphi_l \tag{9}$$

3.4. Mechanisms of Removal. *3.4.1. Diffusion.* The particle concentration decays in a spherical bubble by using one or more of several collection mechanisms, such as impaction, interception, diffusion, electrostatic attraction, condensation, centrifugal force, and gravity. However, diffusion, interception, and impaction are the three primary ones in bubble columns.[18] The theoretical equations were used for predicting the fraction of particles collected in a bubble by considering all three mechanisms. Particle collection by the diffusion mechanism is dominant for submicrometer particle size in bubble scrubbers. Small particles attain a high diffusion coefficient because the diffusion coefficient is inversely proportional to size. The fraction of particles collected in a bubble due to diffusion is given by Fuchs.[18]

$$\eta_{diff} = 3.6\left(\frac{2}{d_b^2}\right)^{1/2} Pe^{-1/2} \tag{10}$$

$$Pe = \frac{d_b v_b}{D_{diff}} \tag{11}$$

where Pe is the Peclet number. For the diffusion coefficient, D_{diff}, appearing in the Peclet number, the following form is used

$$D_{diff} = \frac{kTC}{3\pi\mu d_p} \tag{12}$$

where k is the Boltzmann constant, T the absolute temperature, μ the viscosity of the air, d_p the particle diameter, and C the

dx.doi.org/10.1021/ie3027422 | Ind. Eng. Chem. Res. 2013, 52, 3441−3452

Cunningham slip correction factor. Here the value of C is obtained by the following equation:[19]

$$C = \frac{2(1.664)\lambda}{d_p} \quad d_p \le 0.05\ \mu\text{m} \tag{13a}$$

$$C = \frac{2.069\sqrt{2\lambda}}{d_p^{1/2}} \quad 0.05\ \mu\text{m} \le d_p \le 1\ \mu\text{m} \tag{13b}$$

$$C = 1 \quad d_p > 1\ \mu\text{m} \tag{13c}$$

where λ is the mean free path length of the molecule.

In the case of very small particles whose diameters are smaller than about 0.05 μm, by incorporating eqs 11, 12, and 13, the Peclet number is expressed as

$$Pe = \frac{3\pi\mu d_b v_b}{2(1.664)kT\lambda} d_p^{\,2} \quad d_p \le 0.05\ \mu\text{m} \tag{14a}$$

$$Pe = \frac{3\pi\mu d_b v_b}{2.609kT\sqrt{2\lambda}} d_p^{\,3/2} \quad 0.05\ \mu\text{m} \le d_p \le 1\ \mu\text{m} \tag{14b}$$

$$Pe = \frac{3\pi\mu d_b v_b}{kT} d_p \quad d_p > 1\ \mu\text{m} \tag{14c}$$

where d_b is the bubble diameter and v_b is the bubble rise velocity. Substituting eq 14 into eq 10, the following equations are obtained

$$\eta_{diff} = 5.36\left(\frac{kT\lambda}{\pi\mu d_b^{\,3} v_b}\right)^{1/2} \cdot d_p^{\,-1} \quad d_p \le 0.05\ \mu\text{m} \tag{15a}$$

$$\eta_{diff} = 5.65\left(\frac{kT\lambda^{1/2}}{\pi\mu d_b^{\,3} v_b}\right)^{1/2} \cdot d_p^{\,-3/4} \quad 0.05\ \mu\text{m} \le d_p \le 1\ \mu\text{m} \tag{15b}$$

$$\eta_{diff} = 2.94\left(\frac{kT}{\pi\mu d_b^{\,3} v_b}\right)^{1/2} \cdot d_p^{\,-1/2} \quad d_p > 1\ \mu\text{m} \tag{15c}$$

Particle collection efficiency by diffusion is expected to decrease with increasing velocity of bubbles, as seen in eqs 15a–c.

3.4.2. Interception. Even if the trajectory of a particle does not depart from the streamline, a particle may still be collected when the center of the particle passes within one particle radius from the bubble surface. This phenomenon is known as the interception mechanism of particle removal. The dimensionless parameter describing the interception effect, R, is defined as the ratio of the particle diameter to the bubble diameter:

$$R = \frac{d_p}{d_b} \tag{16}$$

Jung and Lee[20] derived the fraction of particles collected in a bubble due to the interception mechanism:

$$\eta_{int} = \left(\frac{1-\varphi_g}{J}\right)\left\{\left(\frac{R}{1+R}\right) + 2\left(\frac{R}{1+R}\right)^2\right\} \tag{17}$$

where

$$J = 1 - \frac{6}{5}\varphi_g^{\,1/3} + \frac{1}{5}\varphi_g^{\,2}$$

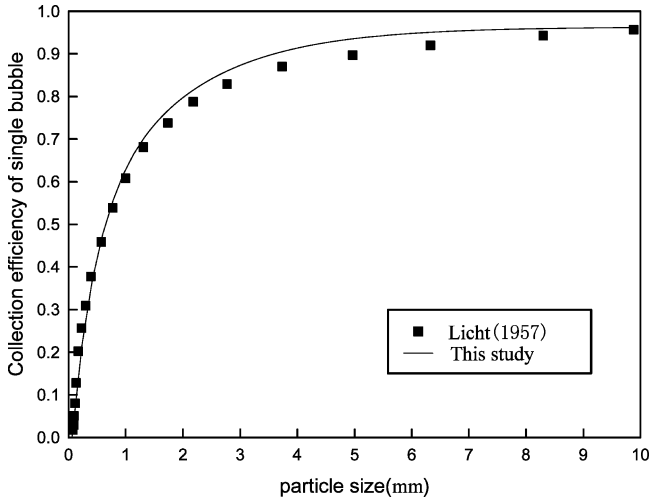

Figure 6. The fraction of particles collected in a bubble due to impaction.

Rearranging for R

$$\eta_{int} = \left(\frac{1-\varphi_g}{J}\right)(R + 2R^2) = \left(\frac{1-\varphi_g}{J}\cdot\frac{1}{d_b}\right)d_p + \left(\frac{1-\varphi_g}{J}\cdot\frac{2}{d_b^{\,2}}\right)d_p^{\,2} \tag{18}$$

where φ_g is the fractional gas holdup.

Interception is relatively independent of flow velocity but increases as the bubble diameter decreases, as seen in eq 18.

3.4.3. Impaction. Impaction is the predominant collection mechanism for scrubbers having gas stream velocities greater than 0.3 m/s[21] or for particles whose diameters are larger than 5.0 μm.[22] The Stokes number, Stk, is the dimensionless parameter indicating the impaction effect and is defined as[23]

$$\text{Stk} = \frac{\rho_p d_p^{\,2} v_h}{9\mu d_b} \tag{19}$$

where ρ_p is the particle density and v_h is the velocity of the tray hole.

For a single bubble, the fraction of particles collected in a bubble due to impaction, η_{imp}, can be written as[23]

$$\eta_{imp} = 0.00376 - 0.0464\text{Stk} + 9.68\text{Stk}^2 - 16.2\text{Stk}^3 \quad 0.0416 \le \text{Stk} \le 0.3 \tag{20a}$$

$$\eta_{imp} = \left(\frac{\text{Stk}}{\text{Stk} + 0.25}\right)^2 \quad \text{Stk} > 0.3 \tag{20b}$$

This form of eq 20b, however, is not suitable for the moment equation used for a log-normal distribution. The collection efficiency due to impaction can be roughly estimated by assuming proportionality to Stk^i. The following equations have been found to approximate eq 20b:

$$\eta_{imp} = 1.52\text{Stk}^{1/3} - 0.45\text{Stk}^{1/2} - 0.54 \quad \text{Stk} > 0.3 \tag{21}$$

With incorporation of eq 19, eqs 20a and 21 become

dx.doi.org/10.1021/ie3027422 | Ind. Eng. Chem. Res. 2013, 52, 3441–3452

$$\eta_{imp} = 0.00376 - 0.0464\frac{\rho_p v_h}{9\mu d_b} d_p^{\ 2} + 9.68\left(\frac{\rho_p v_h}{9\mu d_b}\right)^2 d_p^{\ 4} - 16.2\left(\frac{\rho_p v_h}{9\mu d_b}\right)^3 d_p^{\ 6} \quad 0.0416 \le \mathrm{Stk} \le 0.3 \tag{22a}$$

$$\eta_{imp} = 1.52\left(\frac{\rho_p v_h}{9\mu d_b}\right)^{1/3} d_p^{\ 2/3} - 0.45\left(\frac{\rho_p v_h}{9\mu d_b}\right)^{1/2} d_p - 0.54 \qquad \mathrm{Stk} > 0.3 \tag{22b}$$

The collection efficiency calculated by eqs 22a and 22b is in accordance with Licht,[24] as shown in Figure 6

3.5. Moment Method. The use of moments has the advantage of simplicity in evaluating the continuous evolution of fly ash particles. The three size distribution parameters, namely, the mean particle diameter, the geometric standard deviation, and the total particle number, are allowed to vary during the calculation. This type of representation is widely used in characterization of the time-dependent size distribution of particles in the modeling of aerosols and in comparing experimental data.[25,26]

The kth moment of a particle size distribution is defined as

$$M_k = \int_0^\infty d_p^k n(d_p, t)\, \mathrm{d}d_p \tag{23}$$

while the size distribution function, $n(d_p, t)$, for log-normally distributed particles is defined as

$$n(d_p, t) = \frac{1}{d_p}\frac{N(t)}{\sqrt{2\pi}\ln\sigma_g(t)} \exp\left[-\frac{\ln^2\{d_p/d_g(t)\}}{2\ln^2\sigma_g(t)}\right] \tag{24}$$

where $N(t)$ is the total number concentration of particles, $d_g(t)$ is the geometric number mean particle diameter, and $\sigma_g(t)$ is the geometric standard deviation of particle diameter. Values of d_g and σ_g can be expressed in terms of the first three moments of the distribution as

$$d_g = M_0^{-2/3} M_1^{\ 2} M_2^{-1/2} \tag{25}$$

$$\ln^2\sigma_g = \ln\left(\frac{M_0 M_2}{M_1^{\ 2}}\right) \tag{26}$$

The kth moment of the distribution can be in terms of M_0, d_g, and σ_g

$$M_k = M_0 d_g^k \exp\left(\frac{k^2}{2}\ln^2\sigma_g\right) \tag{27}$$

3.5.1. Diffusion-Dominant Size Regime (d_p <0.05 μm). In the case of very small particles of which diameters are smaller than about 0.05 μm, the overall collection efficiency can be approximately expressed as

$$\eta_{total} = \eta_{diff} = \xi_1 d_p^{\ -1} \tag{28}$$

where

$$\xi_1 = 5.36\left(\frac{kT\lambda}{\pi\mu d_b^{\ 3} v_b}\right)^{1/2}$$

Substituting eq 28 into eq 4b and multiplying both sides by d_p^k and integrating over the entire particle size range, the continuous evolution of the first three moments of the distribution along the tray column is given by

$$\frac{\mathrm{d}M_0}{\mathrm{d}t} = -A\xi_1 M_{-1} = -A(\xi_1 M_0^{\ 3} M_1^{\ -3} M_2^{\ 1}) \tag{29}$$

$$\frac{\mathrm{d}M_1}{\mathrm{d}t} = -A\xi_1 M_0^{\ 1} \tag{30}$$

$$\frac{\mathrm{d}M_2}{\mathrm{d}t} = -A\xi_1 M_1^{\ 1} \tag{31}$$

3.5.2. Intermediate Size Range (0.05 μm < d_p < 5 μm). For the intermediate size range, diffusion, interception, and inertial impaction have to be considered. Thus, the collection efficiency can be written as

$$\eta_{total} = \eta_{diff} + \eta_{int} + \eta_{imp} = \xi_2 d_p^{\ -3/4} + \xi_3 d_p + \xi_4 d_p^{\ 2} + \xi_5 d_p^{\ 4} + \xi_6 d_p^{\ 6} + \xi_7 d_p^{\ 0} \quad 0.05\ \mu\mathrm{m} \le d_p \le 1\ \mu\mathrm{m} \tag{32a}$$

$$\eta_{total} = \eta_{diff} + \eta_{int} + \eta_{imp} = \xi_8 d_p^{\ -1/2} + \xi_3 d_p + \xi_4 d_p^{\ 2} + \xi_5 d_p^{\ 4} + \xi_6 d_p^{\ 6} + \xi_7 d_p^{\ 0} \quad 1\ \mu\mathrm{m} < d_p \le 5\ \mu\mathrm{m} \tag{32b}$$

where

$$\xi_2 = 5.65\left(\frac{kT\lambda^{1/2}}{\pi\mu d_b^{\ 3} v_b}\right)^{1/2}$$

$$\xi_3 = \frac{1-\varphi_g}{J}\cdot\frac{1}{d_b}$$

$$\xi_4 = \frac{1-\varphi_g}{J}\cdot\frac{2}{d_b^{\ 2}} + 0.0464\frac{\rho_p v_h}{9\mu d_b}$$

$$\xi_5 = 9.68\frac{\rho_p v_h}{9\mu d_b}$$

$$\xi_6 = -16.2\frac{\rho_p v_h}{9\mu d_b}$$

$$\xi_7 = 0.00376$$

$$\xi_8 = 2.94\left(\frac{kT}{\pi\mu d_b^{\ 3} v_b}\right)^{1/2}$$

Applying a similar procedure to those used in diffusion-dominant regimes, the following equations are obtained

dx.doi.org/10.1021/ie3027422 | Ind. Eng. Chem. Res. 2013, 52, 3441−3452

$$\frac{dM_0}{dt} = -A(\xi_2 M_{-3/4} + \xi_3 M_1 + \xi_4 M_{-2} + \xi_5 M_4 + \xi_6 M_6 + \xi_7 M_0)$$
$$= -A(\xi_2 {M_0}^{77/32} {M_1}^{-66/32} {M_2}^{21/32} + \xi_3 {M_1}^{1} + \xi_4 {M_2}^{1} + \xi_5 {M_0}^{3} {M_1}^{-8} {M_2}^{6} + \xi_6 {M_0}^{10} {M_1}^{-24} {M_2}^{15} + \xi_7 {M_0}^{1}) \quad (33)$$

$$\frac{dM_1}{dt} = -A(\xi_2 M_{-1/4} + \xi_3 M_2 + \xi_4 M_{-1} + \xi_5 M_5 + \xi_6 M_7)$$
$$= -A(\xi_2 {M_0}^{21/32} {M_1}^{14/32} {M_2}^{-3/32} + \xi_3 {M_2}^{1} + \xi_4 {M_0}^{1} {M_1}^{-3} {M_2}^{3} + \xi_5 {M_0}^{6} {M_1}^{-15} {M_2}^{10} + \xi_6 {M_0}^{15} {M_1}^{-35} {M_2}^{21} + \xi_7 {M_1}^{1}) \quad (34)$$

$$\frac{dM_2}{dt} = -A(\xi_2 M_{5/4} + \xi_3 M_3 + \xi_4 M_4 + \xi_5 M_6 + \xi_6 M_8)$$
$$= -A(\xi_2 {M_0}^{-3/32} {M_1}^{30/32} {M_2}^{5/32} + \xi_3 {M_0}^{1} {M_1}^{-3} {M_2}^{3} + \xi_4 {M_0}^{3} {M_1}^{-8} {M_2}^{6} + \xi_5 {M_0}^{10} {M_1}^{-24} {M_2}^{15} + \xi_6 {M_0}^{21} {M_1}^{-48} {M_2}^{28} + \xi_7 {M_2}^{1}) \quad (35)$$

The first three moments of the distribution are also obtained by the same procedure for 1 μm < $d_p \leq 5$ μm.

3.5.3. Inertial Impaction-Dominant Size Range (d_p >5 μm). In the inertial impaction-dominant size range, the effect of diffusion and interception can be neglected, as shown below

$$\eta_{total} = \eta_{imp} = \xi_9 {d_p}^{2} + \xi_6 {d_p}^{4} + \xi_7 {d_p}^{0} \quad 0.0416 \leq \text{Stk} \leq 0.3 \quad (36a)$$

$$\eta_{total} = \eta_{imp} = \xi_{10} {d_p}^{2/3} + \xi_{11} {d_p}^{1} + \xi_{12} {d_p}^{0} \quad \text{Stk} > 0.3 \quad (36b)$$

where

$$\xi_9 = 0.0464 \frac{\rho_p v_h}{9\mu d_b}$$

$$\xi_{10} = 1.52 \left(\frac{\rho_p v_h}{9\mu d_b} \right)^{1/3}$$

$$\xi_{11} = -0.45 \left(\frac{\rho_p v_h}{9\mu d_b} \right)^{1/2}$$

$$\xi_{12} = -0.54$$

By substituting eq 36a into eq 4b, the following equations are obtained:

$$\frac{dM_0}{dt} = -A(\xi_9 M_2 + \xi_6 M_4 + \xi_7 M_0)$$
$$= -A(\xi_9 {M_2}^{1} + \xi_6 {M_0}^{3} {M_1}^{-8} {M_2}^{6} + \xi_7 {M_0}^{1}) \quad (37)$$

$$\frac{dM_1}{dt} = -A(\xi_9 M_3 + \xi_6 M_5 + \xi_7 M_1)$$
$$= -A(\xi_9 {M_0}^{1} {M_1}^{-3} {M_2}^{3} + \xi_6 {M_0}^{6} {M_1}^{-15} {M_2}^{10} + \xi_7 {M_1}^{1}) \quad (38)$$

$$\frac{dM_1}{dt} = -A(\xi_9 M_4 + \xi_6 M_6 + \xi_7 M_2)$$
$$= -A(\xi_9 {M_0}^{3} {M_1}^{-8} {M_2}^{6} + \xi_6 {M_0}^{10} {M_1}^{-24} {M_2}^{15} + \xi_7 {M_2}^{1}) \quad (39)$$

The first three moments of the distribution are also obtained by the same procedure for Stk > 0.3.

Equations 29−31, 33−35, or 37−39, along with the initial conditions, constitute a set of coupled ordinary differential equations that describe the continuous evolution of the first three moments of the distribution. These equations can be solved by the fourth-order Runge−Kutta method.

4. RESULTS AND DISCUSSION

Gas holdup, one of the most important parameters, has been discussed in many research papers.[27,28] In the present work, the clear liquid height and froth height were experimentally determined to calculate the gas holdup using eq 7. The experimental values of the froth height H_F for the fixed valve tray are shown in Figure 7. At the working condition of negligible weeping and entrainment, H_F is determined by the gas and liquid volume rate and the tray geometry, as shown in Figure 7. This is consistent with most conclusions drawn by other researchers in the literature.[29]

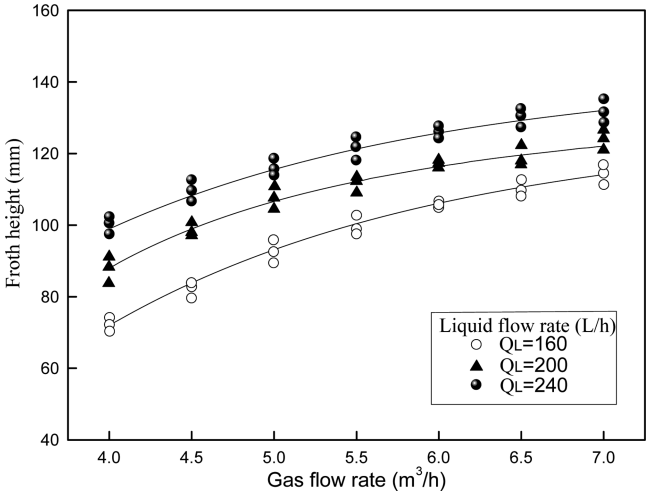

Figure 7. The effect of gas flow rate on froth height at different liquid flow rates.

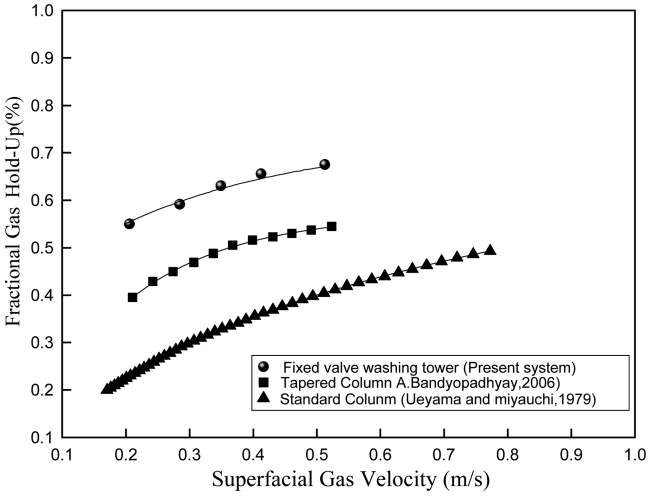

Figure 8. Effect of superficial gas velocity on fractional gas holdup.

The following correlation, referred from the literature,[28] is appropriate for the fixed valve trays

dx.doi.org/10.1021/ie3027422 | Ind. Eng. Chem. Res. 2013, 52, 3441−3452

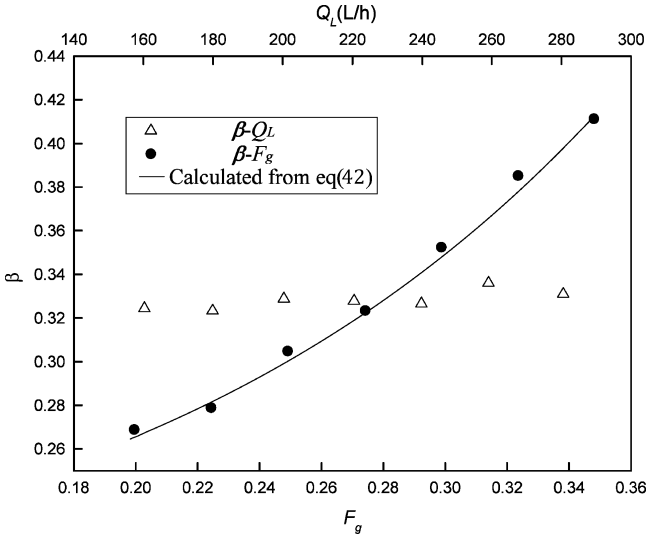

Figure 9. β values as a function of F_g factors and liquid flow rate.

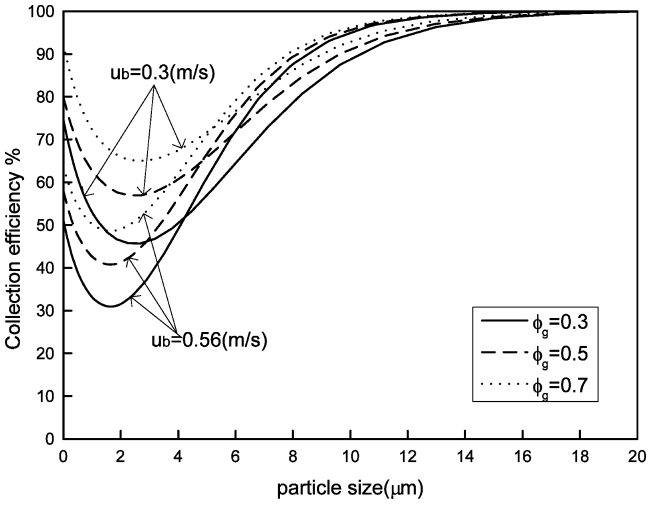

Figure 10. Collection efficiency of fly ash particles for different bubble slip velocities and the same bubble size (d_b = 8 mm).

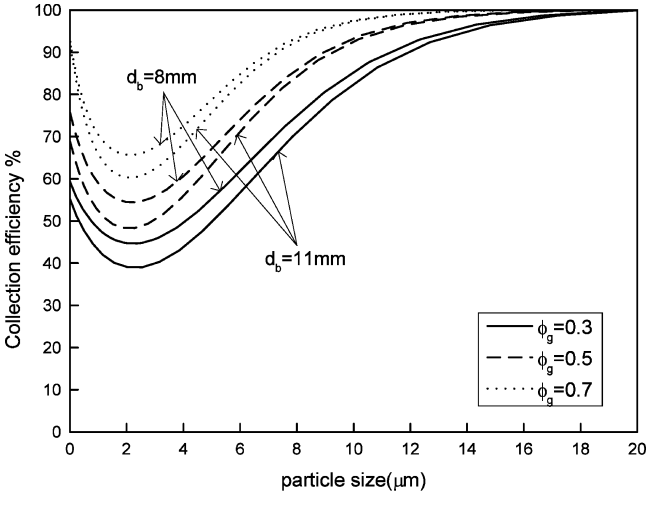

Figure 11. Collection efficiency of fly ash particles for different bubble sizes and the same bubble velocity (v_b = 0.3 m/s).

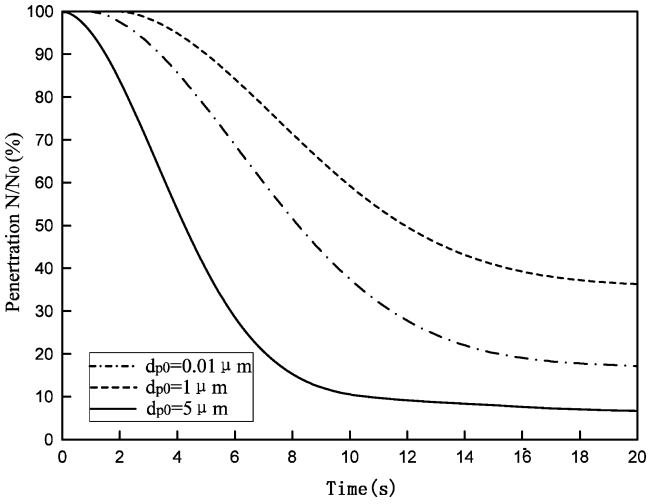

Figure 12. Penetration of fly ash particles in different geometric mean diameters.

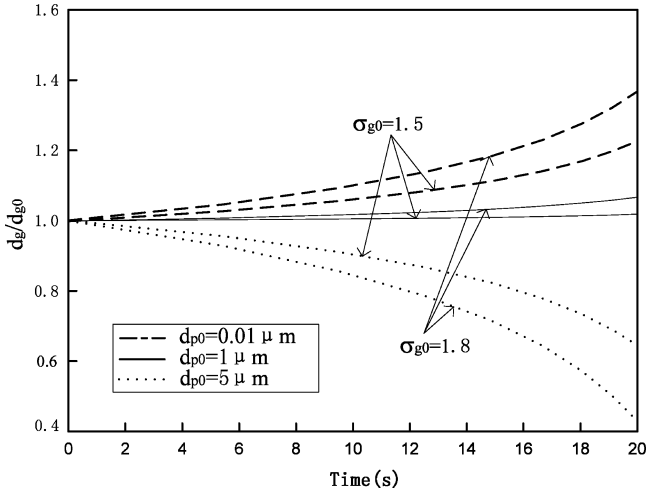

Figure 13. Geometric mean diameter of fly ash particle size distribution in the diffusion-dominant region (d_{pg0} = 0.01 μm), intermediate region (d_{pg0} = 1 μm), and impaction-dominant region (d_{pg0} = 5 μm).

$$H_F = \frac{4.8 v_g^{0.79}}{d_0^{0.14} \phi^{1.9}} \left(\frac{Q_L}{Q_g} \right)^{0.2} \quad (40)$$

where Q_L/Q_g is the liquid−gas ratio (L/m^3), d_0 the hole diameter (m), and ϕ the ratio of perforation area to tray area.

The experimental values of gas holdup are shown in Figure 8. It can be seen from the figure that the fractional gas holdup is gradually increasing with the superficial gas velocity. The data of the present system are also compared with the data reported in the literature[30] for gas holdup against superficial gas velocity measured for the air−water system in standard bubble columns with circular cross-section and tapered column. It shows that the present system offers relatively higher holdup than the existing systems under similar situations. The dependence of the gas holdup on superficial gas velocity in the present system is found to be of the following form:[31]

$$\varphi_g = 1 - \exp(-0.45 - 0.59\sqrt{F_g}) \quad (41)$$

dx.doi.org/10.1021/ie3027422 | Ind. Eng. Chem. Res. 2013, 52, 3441−3452

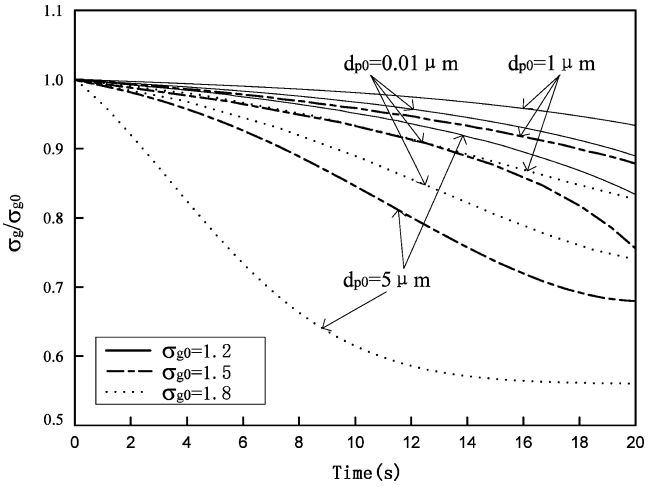

Figure 14. Geometric standard deviation of fly ash particle size distribution in the diffusion-dominant region (d_{pg0} = 0.01 μm), intermediate region (d_{pg0} = 1 μm), and impaction-dominant region (d_{pg0} = 5 μm).

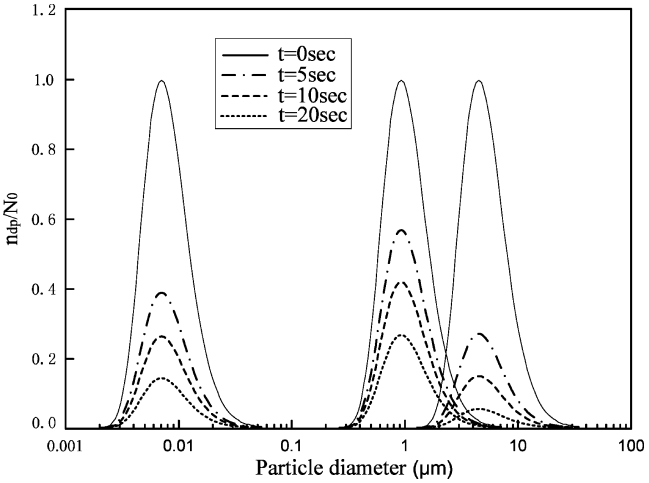

Figure 15. The evolution of fly ash particle size distribution in the diffusion-dominant region (d_{pg0} = 0.01 μm), intermediate region (d_{pg0} = 1 μm), and impaction-dominant region (d_{pg0} = 5 μm).

The parameter β can be easily and directly calculated from the experimental values of bubble size using eq 8, as illustrated in Figure 9 that β decreases with the increasing F factor and depends quite weakly on the liquid flow rate.

Even though β is the function of C_d, C_n, and We_{crit}, as shown in eq 8, C_n and We_{crit} usually behave to be constants, or of small deviations as pointed out in most papers.[32] Therefore, the decreasing β with the increasing F_g is attributed to the dependence of C_d on F_g and the regressive expression of β can be obtained as

$$\beta = 8.51F_g^{0.7729} \tag{42}$$

Combining eq 42 with eq 8,

$$d_b = 8.51F_g^{0.7729}\left(\frac{\sigma}{\rho_L}\right)^{3/5}(u_g g)^{-2/5} \tag{43}$$

The collection efficiency of the fixed valve tray scrubber can be changed when operational conditions such as the bubble velocity, bubble size, and gas holdup are varied. Figure 10 shows the collection efficiency of fly ash particles for different bubble slip velocities at a gas flow rate of 5 m^3/h, a liquid flow rate of 200 L/h, and an inlet particle loading of 30 g/m^3. It is shown in Figure 10 that the collection efficiency curves significantly move to the upper right as the velocity of rising bubble decreases. This means that a decrease in the velocity of a rising bubble can help collect small particles, but it prevents large particles from being captured.

For particles larger than 5 μm, inertial impaction plays an important role. The increase of bubble velocity will increase the momentum of particles. Therefore, particles will be more likely to be carried into the liquid. For particles finer than 3 μm, the collection efficiency of fly ash decreases with the increase in bubble velocity. This is because the diffusion mechanism is very much dependent on residence time, and the particle size. As the particle size decreases and the particle residence time increases, the diffusive mechanism becomes more important. Small particles attain a high diffusion coefficient because the diffusion coefficient is inversely proportional to size, and the particle residence time increases will enhance the probability of particle−bubble surface collisions in the washing column. Increasing the bubble velocity results in a shorter residence time in the scrubber. Consequently, the removal efficiency will decrease by decreasing the residence time of the particles smaller than 3 μm.

Bubble size also plays a significant role in the scrubber collection efficiency. One of the most important design implications of a tray column scrubber is the bubble size. Figure 11 shows the collection efficiency of fly ash particles for different bubble sizes at gas flow rates of 5 m^3/h, liquid flow rates of 200 L/h, and inlet particle loadings of 30 g/m^3. It is shown in Figure 11 that particle collection efficiencies are enhanced for the entire particle size range as the bubble size decreases. The radius of curvature of the bend in the streamline has a very important effect on the probability that a particle will be carried into the liquid. The smaller the radius of curvature, the less likely that a particle will follow the streamline. Therefore, small bubbles are more likely to be impacted than large bubbles. To achieve better removal efficiency of fine particles as well as the overall removal efficiency, it is suggested to decrease the bubble size.

From Figures 10 and 11, one can also recognize that, for the same gas and liquid flow rate, the collection efficiency will increase with gas holdup. As the gas holdup increases, the intensity of bubble bursting, regeneration, and rebursting which enhances the probability of interparticle and particle−bubble surface collisions in the washing column.[17]

The penetration of particles as a function of time was calculated with three fly ash particles for comparison. Their geometric mean diameters were 0.01, 1.0, and 5.0 μm, respectively, but standard deviations were the same at 1.5. Figure 12 shows the penetration of fly ash particles in different geometric mean diameters at a gas flow rate of 5 m^3/h, a liquid flow rate of 200 L/h, and an inlet particle loading of 30 g/m^3. In the case of the geometric mean particle diameter of 0.01 μm, the diffusion mechanism is dominant, while, for the case of a geometric mean diameter of 1.0 μm, a region exists where the impaction and the diffusion are minimum. The minimum is called the most penetrating particle size region. Thus, particles having a diameter of 5 μm are removed faster than those with a diameter of 1.0 μm.

The three size distribution parameters of fly ash particles may change in the course of scrubbing. To obtain information on

dx.doi.org/10.1021/ie3027422 | Ind. Eng. Chem. Res. 2013, 52, 3441−3452

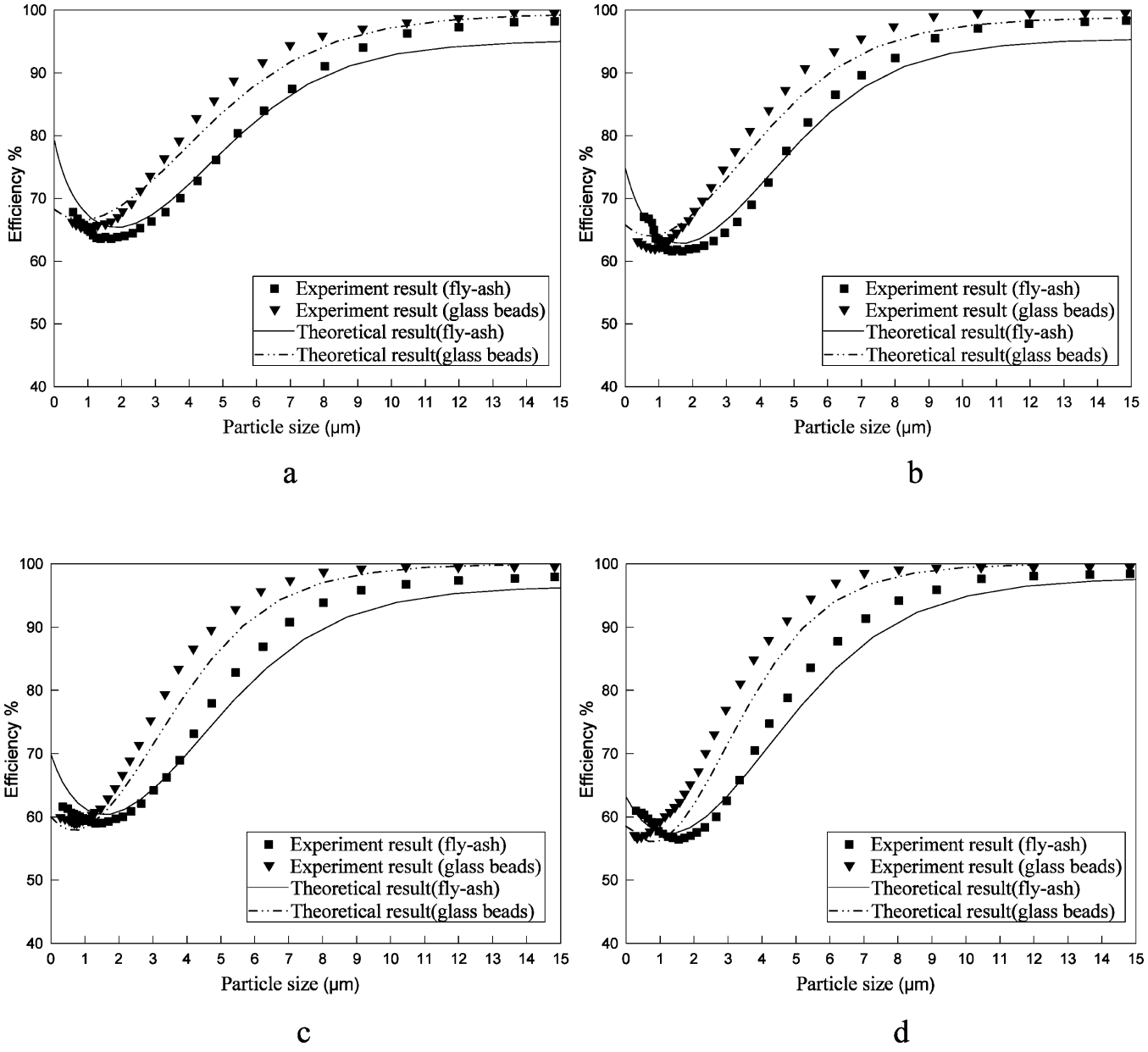

Figure 16. Comparison of theoretical and experimental results of fly ash and glass beads. Gas flow rate: (a) 4 m^3/h, (b) 5 m^3/h, (c) 6 m^3/h, and (d) 7 m^3/h.

them, the three ordinary differential equations shown in eqs 29−31, eqs 33−35, or eqs 37−39 were applied. Figures 13 and 14 are the geometric mean diameter and the geometric standard deviation, respectively. Each curve in these figures has been obtained for a fixed gas flow rate of 5 m^3/h, aliquid flow rate of 160 L/h, and an inlet particle loading of 30 g/m^3. Figure 13 shows two different tendencies of geometric mean diameters. The mean diameter of fly ash particles in the diffusion-dominant region increases in the course of scrubbing, whereas in the impaction-dominant region it decreases. This is clearly because the collection efficiency curve is parabolic, as mentioned above. That means the collection efficiencies of fly ash particles both in the diffusion and in the impaction-dominant regions are higher than that in the intermediate region. Figure 14 shows all of the geometric standard deviations for fly ash particles decrease in time, but the standard deviation of fly ash in the impaction-dominant region decreases at a higher rate than that in the diffusion-dominant region and the intermediate region.

Figure 15 represents the evolution of fly ash particle size distribution in the diffusion-dominant region, intermediate region, and impaction-dominant region at a gas flow rate of 5 m^3/h, a liquid flow rate of 160 L/h, and an inlet particle loading of 30 g/m^3. The particle size distribution shows the decrease in the total number of fly ash particles in the impaction-dominant region at a higher rate compared with fly ash in the diffusion-dominant region and the intermediate region.

Figure 16 represents the obtained results of the effect of particle size on collection efficiency at different gas flow rates, a constant liquid flow rate of 200 L/h, and an inlet particle loading of 30 g/m^3. It shows that the predicted results of this study are in good accordance with the experimental results at all operation conditions. For particles larger than 3 μm of fly ash and 1 μm of glass beads, as the particle size increases, the

dx.doi.org/10.1021/ie3027422 | Ind. Eng. Chem. Res. 2013, 52, 3441−3452

collection efficiency increases steadily and reaches the maximum nearly 100% for particles of 15 μm at a gas flow rate of 4 m^3/h and a liquid flow rate of 200 L/h.

The collection efficiency of fly ash is considerably lower than that of glass beads for the particle size range 1−10 μm, while for particles finer than 1 μm the collection efficiency of fly ash is higher than that of glass beads. For the same particle size, the mass of glass beads is larger than fly ash, and therefore, the momentum of glass beads is larger than that of fly ash, which causes particles to travel in a straight line toward the bubble surface. The particle leaves the streamline as the streamline bends to move around the bubble surface. The greater the mass of the particle, the more likely that it will travel in a straight line. Thus, glass beads are more likely to be carried into the liquid than fly ash. Meanwhile, it was observed that hydrophilic, easily wettable particles are removed more completely by wet methods than the hydrophobic ones.[33] For particles larger than 10 μm, the collection efficiencies of two kinds of particles are almost the same; this is because the wettability of particles plays the lesser role when the particle size is increasing and does not affect the collection efficiency for particles larger than 10 μm;[34] therefore, the addition of surfactants to water is useless.

5. CONCLUSIONS

In this study, the characterization of time-dependent size distribution and collection efficiency of particles in a fixed valve bubble column were investigated, varying several operation conditions such as bubble velocity, bubble size, gas holdup, and particle wettability. The theoretical results were compared with the results of experiment. The results drawn from this study can be summarized as follows:

(1) The geometric standard deviations of particle size distribution decrease as fly ash particles pass through the fixed valve column. The geometric mean diameter of fly ash particles in the diffusion-dominant region increases, whereas that in the impaction-dominant region decreases.

(2) Bubble velocity, bubble size, and gas holdup play an important role in determining the particle collection efficiency of bubble columns. The collection efficiency is enhanced in the entire particle size range either as bubble size decreases or as gas holdup increases.

(3) The predicted collection efficiencies of this study are in a good accordance with the experimental efficiencies in all operation conditions. The collection efficiency is represented as a U-shaped curve with a minimum in the region of around 2.0 μm in particle diameter. Fly ash collection efficiency is considerably lower than that of glass beads in the particle size range 1−10 μm, while for particles larger than 10 μm the collection efficiency of two kinds of particles are almost the same.

AUTHOR INFORMATION

Corresponding Author

*Fax: +86 21 64251312. Tel.: +86 21 64250734. E-mail: cxl@ecust.edu.cn.

Notes

The authors declare no competing financial interest.

ACKNOWLEDGMENTS

This research was supported by Program for New Century Excellent Talents in University of China (NCET-12-0854) and National High-tech R&D Program of China (2007AA050301, 2012AA053101).

REFERENCES

(1) Sharma, S.; Dolan, M.; Park, D.; Morpeth, L.; Ilyushechkin, A.; McLennan, K.; Harris, D.; Thambimuthu, K. A critical review of syngas cleaning technologies—fundamental limitations and practical problems. *Powder Technol.* **2008**, *180* (1), 115−121.

(2) Cui, J.; Chen, X.; Gong, X.; Yu, G. Numerical Study of Gas−Solid Flow in a Radial-Inlet Structure Cyclone Separator. *Ind. Eng. Chem. Res.* **2010**, *49* (11), 5450−5460.

(3) Yoshida, H.; Ono, K.; Fukui, K. The effect of a new method of fluid flow control on submicron particle classification in gas-cyclones. *Powder Technol.* **2005**, *149* (2), 139−147.

(4) Wark, K.; Warner, G. F.; Davis, W. T. Particulate Control. In *Air Pollution: Its Origin and Control*, 3rd ed.; Addison-Wesley: Menlo Park, 1998; p 278.

(5) Dullien, F. A. L. *Introduction to industrial gas cleaning*; Academic Press: San Diego, CA, 1989; pp 55−90.

(6) Lee, B. K.; Jung, K. R.; Park, S. H. Development and application of a novel swirl cyclone scrubber—(1) Experimental. *J. Aerosol Sci.* **2008**, *39* (12), 1079−1088.

(7) Bandyopadhyay, A.; Biswas, M. N. Particulate scrubbing in a novel two-stage hybrid scrubber. *AIChE J.* **2006**, *52* (2), 850−854.

(8) Kaldor, T. G.; Phillips, C. R. Aerosol Scrubbing by Foam. *Ind. Eng. Chem. Process Des. Dev.* **1976**, *15* (1), 199−206.

(9) Park, S. H.; Lee, B. K. Development and application of a novel swirl cyclone scrubber:(2) Theoretical. *J. Hazard. Mater.* **2009**, *164* (1), 315−321.

(10) Meikap, B.; Kundu, G.; Biswas, M. Modeling of a novel multi-stage bubble column scrubber for flue gas desulfurization. *Chem. Eng. J.* **2002**, *86* (3), 331−342.

(11) Meikap, B.; Biswas, M. Fly-ash removal efficiency in a modified multi-stage bubble column scrubber. *Sep. Purif. Technol.* **2004**, *36* (3), 177−190.

(12) Wang, Q.; Chen, X.; Gong, X. Theoretical and experimental investigation on the characteristics of fly-ash scrubbing in a fixed valve tray column. *AIChE J.* **2012**, DOI: 10.1002/aic.13967.

(13) Kemoun, A.; Rados, N.; Li, F.; Al-Dahhan, M.; Dudukovic, M.; Mills, P.; Leib, T.; Lerou, J. Gas holdup in a trayed cold-flow bubble column. *Chem. Eng. Sci.* **2001**, *56* (3), 1197−1205.

(14) Revankar, S.; Ishii, M. Local interfacial area measurement in bubbly flow. *Int. J. Heat Mass Transfer* **1992**, *35* (4), 913−925.

(15) Hesketh, R.; Fraser Russell, T.; Etchells, A. Bubble size in horizontal pipelines. *AIChE J.* **2004**, *33* (4), 663−667.

(16) Liang, Y. C.; Zhou, Z.; Shao, M.; Geng, J.; Wu, Y. T.; Zhang, Z. B. The impact of valve tray geometry on the interfacial area of mass transfer. *AIChE J.* **2008**, *54* (6), 1470−1477.

(17) Bandyopadhyay, A.; Biswas, M. Fly-ash scrubbing in a tapered bubble column scrubber. *Process Saf. Environ. Prot.* **2006**, *84* (1), 54−62.

(18) Fuchs, N. A. *The Mechanics of Aerosols*; Pergamon Press: New York, 1964.

(19) Lee, K.; Liu, B. On the minimum efficiency and the most penetrating particle size for fibrous filters. *J. Air Pollut. Control Assoc.* **1980**, *30* (4), 377−381.

(20) Jung, C.; Lee, K. Filtration of fine particles by multiple liquid droplet and gas bubble systems. *Aerosol Sci. Technol.* **1998**, *29* (5), 389−401.

(21) Cheng, L. Collection of airborne dust by water sprays. *Ind. Eng. Chem. Process Des. Dev.* **1973**, *12* (3), 221−225.

(22) Kim, H.; Jung, C.; Oh, S.; Lee, K. Particle removal efficiency of gravitational wet scrubber considering diffusion, interception, and impaction. *Environ. Eng. Sci.* **2001**, *18* (2), 125−136.

(23) Fonda, A.; Herne, H. The classical computation of the aerodynamic capture of particle by spheres. *Int. J. Air Pollut.* **1960**, *3*, 26.

(24) Licht, W. *Air pollution control engineering: Basic calculations for particulate collection*, 2nd ed.; Marcel Dekker: NewYork, 1998; p 216.

(25) Jung, C. H.; Kim, Y.; Lee, K. Analytic solution for polydispersed aerosol dynamics by a wet removal process. *J. Aerosol Sci.* **2002**, *33* (5), 753−767.
(26) Lim, K.; Lee, S.; Park, H. Prediction for particle removal efficiency of a reverse jet scrubber. *J. Aerosol Sci.* **2006**, *37* (12), 1826−1839.
(27) Jaćimović, B.; Genić, S. B. Froth porosity and clear liquid height in trayed columns. *Chem. Eng. Technol.* **2000**, *23* (2), 171−176.
(28) Kemoun, A.; Rados, N.; Li, F.; Al-Dahhan, M.; Dudukovic, M.; Mills, P.; Leib, T.; Lerou, J. Gas holdup in a trayed cold-flow bubble column. *Chem. Eng. Sci.* **2001**, *56* (3), 1197−1205.
(29) Wang, S. H. *Petrochemical Engineering Design Handbook*; Chemical Industry Publishing Company: Beijing, 2002; p 324.
(30) Shah, Y.; Kelkar, B. G.; Godbole, S.; Deckwer, W. D. Design parameters estimations for bubble column reactors. *AIChE J.* **1982**, *28* (3), 353−379.
(31) *Bubble-Tray Design Manual*; AIChE: New York, 1958.
(32) Rigby, G.; Evans, G.; Jameson, G. Bubble breakup from ventilated cavities in multiphase reactors. *Chem. Eng. Sci.* **1997**, *52* (21), 3677−3684.
(33) Taheri, M.; Calvert, S. Removal of small particles from air by foam in a sieve-plate column. *J. Air Pollut. Control Assoc.* **1968**, *18* (4), 240−245.
(34) Stulov, L.; Murashkevich, F.; Fuchs, N. The efficiency of collision of solid aerosol particles with water surfaces. *J. Aerosol Sci.* **1978**, *9* (1), 1−6.